



Self-feeding paper based biofuel cell/self-powered hybrid  $\mu$ -supercapacitor integrated system / Narvaez Villarrubia, Claudia W.; Soavi, Francesca; Santoro, Carlo; Arbizzani, Catia; Serov, Alexey; Rojas-Carbonell, Santiago; Gupta, Gautam; Atanasov, Plamen. - In: BIOSENSORS & BIOELECTRONICS. - ISSN 0956-5663. - STAMPA. - 86:(2016), pp. 459-465. [[10.1016/j.bios.2016.06.084](https://doi.org/10.1016/j.bios.2016.06.084)]

## Alma Mater Studiorum Università di Bologna Archivio istituzionale della ricerca

Self-feeding paper based biofuel cell/self-powered hybrid  $\mu$ -supercapacitor integrated system

This is the final peer-reviewed author's accepted manuscript (postprint) of the following publication:

*Published Version:*

*Availability:*

This version is available at: <https://hdl.handle.net/11585/566732> since: 2022-01-21

*Published:*

DOI: <http://doi.org/10.1016/j.bios.2016.06.084>

*Terms of use:*

Some rights reserved. The terms and conditions for the reuse of this version of the manuscript are specified in the publishing policy. For all terms of use and more information see the publisher's website.

This item was downloaded from IRIS Università di Bologna (<https://cris.unibo.it/>).  
When citing, please refer to the published version.

(Article begins on next page)

This is the final peer-reviewed accepted manuscript of:

**C. W.Narvaez Villarrubia, F. Soavi \*, C Santoro, C. Arbizzani, A. Serov, S. Rojas-Carbonell, G. Gupta, P. Atanassov\*, Self-feeding paper based biofuelcell/self-powered hybrid  $\mu$ -supercapacitor integrated system, Biosensors and Bioelectronics 86 (2016) 459–465.**

The final published version is available online at:  
<https://doi.org/10.1016/j.bios.2016.06.084>

Rights / License:

The terms and conditions for the reuse of this version of the manuscript are specified in the publishing policy. For all terms of use and more information see the publisher's website.

*This item was downloaded from IRIS Università di Bologna (<https://cris.unibo.it/>)*

***When citing, please refer to the published version.***

1 **Self-Feeding Paper Based Biofuel Cell / Self-Powered hybrid  $\mu$ -supercapacitor**  
2 **integrated system**

3

4 Claudia W. Narvaez Villarrubia<sup>1,a</sup>, \*Francesca Soavi<sup>2,a</sup>, Carlo Santoro<sup>3,a</sup>, Catia Arbizzani<sup>2</sup>,  
5 Alexey Serov<sup>3</sup>, Santiago Rojas-Carbonell<sup>3</sup>, Gautam Gupta<sup>1</sup>, \*\*Plamen Atanassov<sup>3</sup>.

6

7 <sup>1</sup> MPA-11 Material Synthesis and Integrated Devices, Los Alamos National Laboratory,  
8 Los Alamos, NM, USA

9 <sup>2</sup> Department of Chemistry “Giacomo Ciamician”, Alma Mater Studiorum - Università di  
10 Bologna, Via Selmi, 2, 40126 Bologna, Italy

11 <sup>3</sup> Center Micro-Engineered Materials (CMEM), Department of Chemical and Biological  
12 Engineering, University of New Mexico, NM, USA

13

14 <sup>a</sup> the three authors have contributed equally to the manuscript

15

16 **\*corresponding authors**

17

18 \* Francesca Soavi, Department of Chemistry “Giacomo Ciamician”, Alma Mater  
19 Studiorum-Università di Bologna, Via Selmi, 2, Bologna, Italy, e-mail:

20 francesca.soavi@unibo.it

21

22 \*\* Plamen Atanassov, Center for Micro-Engineered Materials (CMEM), Department of  
23 Chemical & Biological Engineering, University of New Mexico, Albuquerque, NM 87131,  
24 USA, e-mail: plamen@unm.edu

25

26 **Abstract**

27

28 For the first time, a paper based enzymatic fuel cell is used as self-recharged  
29 supercapacitor. In this supercapacitive enzymatic fuel cell (SC-EFC), the supercapacitive  
30 features of the electrodes are exploited to demonstrate high power output under pulse  
31 operation. Glucose dehydrogenase-based anode and bilirubin oxidase-based cathode were  
32 assembled to a quasi-2D capillary-driven microfluidic system. Capillary flow guarantees  
33 the continuous supply of glucose, cofactor and electrolytes to the anodic enzyme and the  
34 gas-diffusional cathode design provides the passive supply of oxygen to the catalytic layer  
35 of the electrode. The paper-based cell was self-recharged under rest and discharged by high  
36 current pulses up to  $4 \text{ mA cm}^{-2}$ . The supercapacitive behavior and low equivalent series  
37 resistance of the cell permitted to achieve up to a maximum power of  $0.87 \text{ mWcm}^{-2}$  ( $10.6$   
38  $\text{mW}$ ) for pulses of  $0.01 \text{ s}$  at  $4 \text{ mA cm}^{-2}$ . This operation mode allowed the system to achieve  
39 at least one order of magnitude higher current/power generation compared to the steady  
40 state operation. Three days durability tests (4200 cycles) were run at current pulses of  $0.4$   
41  $\text{mAcm}^{-2}$ . Results showed a slight decrease in working open circuit voltage (OCV) and a  
42 decrease of cell capacitance during the operations.

43

44 **Keywords:** Enzymatic Fuel Cell, Supercapacitor, paper-based microfluidic system, power  
45 pulses

46

## 47 **1. Introduction**

48

49 Enzymatic fuel cells (EFC) are energy and power harvesting devices, theoretically,  
50 capable to obtain high power density from biofuels at circum-neutral pH. However, actual  
51 power and energy density is lower than theoretical performance (Minteer et al., 2007; Davis  
52 et al.; 2007; Yu and Scott, 2010; Falk et al., 2013; Cosnier et al., 2014; Slaughter et al.  
53 2015). Optimum power/energy harvesting still remains a challenge to overcome when  
54 compared to commercial batteries and conventional fuel cells (FCs). Consequently, an  
55 improved internal design and its integration with other electrochemical devices such as a  
56 supercapacitor seems to be appropriate for enhancing the performance up to the level  
57 required to power small portable devices or biomedical devices (Southcott et al., 2013,  
58 Narváez Villarrubia et al., 2014; Pankratov et al., 2016; Kizling et al., 2015).

59 Redox enzymes are employed for enzymatic fuel cell (EFC) applications to harvest  
60 energy from biofuels found in nature (Minteer et al., 2007; Davis et al.; 2007; Yu and Scott,  
61 2010; Falk et al., 2013; Cosnier et al., 2014). These enzymes are specific for catalyzing the  
62 reduction or oxidation of their substrates, offering a high theoretical efficiency, leaving no  
63 toxic residues of reaction (Sokic-Lazic et al., 2008; Gellett et al., 2010; González-Guerrero  
64 et al.; 2013; Tam et al., 2009; Amir et al., 2009). Enzymatic fuel cells offer the capability  
65 to operate at room temperature and neutral pH, conditions which cannot be achieved by  
66 conventional FCs (Heller, 1992; Mano et al., 2003; Soukharev et al., 2004; Kang et al.,

67 2006). Even though these devices provide several advantages, the effect of various limiting  
68 factors on the system result in low power output generation. Stability of the enzymes  
69 outside their natural environment, the partial oxidation of the substrates and transport of  
70 biofuels to the catalytic sites of the electrodes are factors limiting the performance of EFCs.  
71 Certain criteria to mitigate the limiting factors mentioned above need to be satisfied to  
72 improve efficiency (Pardo-Yissar et al., 2000; Tarasevich et al., 2002; Moore et al., 2005;  
73 Atanassov et al., 2007; Cooney et al., 2008; Ivnitski et al., 2008; Gupta et al., 2009; Rincon  
74 et al., 2011; Minteer, 2012a; Minteer et al., 2012b; Reid et al., 2013; Rasmussen et al.  
75 2016). In Addition, the need of an efficient transport of fuel to the catalytic sites should be  
76 addressed.

77 Our group addressed those issues, in previous research, constructing a  
78 biodegradable EFC that independently powered a small device for 36 hours (Ciniciato et  
79 al., 2012; Narvaez Villarrubia et al., 2014) and, later, used an enzymatic cascade system  
80 working with ethanol and methanol (Lau et al., 2015). The catalytic layer was designed to  
81 enhance enzyme loading and stability using a highly porous and conductive bucky-paper  
82 (multiwall carbon nanotubes (MWCNTs)-based paper). Also, a cellulose paper-based  
83 quasi-2D microfluidic system was utilized to self-transport fuel to the catalytic layer on the  
84 electrodes as well as to work as proton exchange membrane, electrode separator and  
85 structural mechanical support. This self-fed EFC design offered the possibility to power  
86 small devices utilizing ubiquitous fuels, and simultaneously addressing environmental  
87 concerns. Assembling this EFC to a supercapacitor could enhance its performance to  
88 achieve energy/power demand of small devices for various applications. Several studies  
89 have shown paper-based systems feasibly used to develop bioelectrodes and microfluidic

90 systems mainly for biosensors or EFC to power biosensors (Shitanda et al. 2013; Strack et  
91 al. 2013; Li et al. 2015; Reid et al. 2015; Slaughter et al. 2016; Majdecka et al. 2016;  
92 Desmet et al. 2016). Powering small portable or medical devices that demand higher  
93 energy/power is a challenge to overcome by designing hybrid systems.

94       Supercapacitors are high power electrochemical energy storage systems with high  
95 capacitance electrodes that can be charged and discharged through fast and reversible  
96 processes (Beguin et al.; 2014; Conway, 1999). They are considered the most suitable  
97 devices for high power pulse delivery. Examples of hybrid bio-devices integrating  
98 supercapacitors such as bio-batteries and biosensors, utilizing enzymatic systems, were  
99 developed by Skunik-Nuckowska *et al.* (2014) and Kizling *et al.* (2015), respectively. The  
100 integration of internal supercapacitors within biofuel cells has been shown in previous  
101 studies by Pankratov *et al.* (2014a; 2014b; 2014c), by González-Arribas *et al.* (2016) and  
102 by Agnes *et al.* (2014).

103       Pankratov *et al.* have developed, for the first time, a self-charging bio-capacitor  
104 using cellobiose dehydrogenase (CDH) and bilirubin oxidase (BOx) as anodic and  
105 enzymatic systems, respectively, where the electrochemical capacitor and the EFC function  
106 simultaneously (Pankratov *et al.* 2014a; 2014c). Higher power pulses were obtained by  
107 Agnès *et al.* (2014). They used glucose oxidase (GOx) and catalase enzymes at the anode  
108 and laccase at cathode, correspondingly. Both anodic and cathodic enzymatic systems were  
109 entrapped in carbon nanotubes (CNTs)-based matrix conforming pellet-like bio-electrodes.  
110 The bio-electrodes were immersed into an electrolytic solution containing glucose and  
111 oxygen that was actively supplied by a pump (air saturated solution). The open circuit  
112 potential was roughly 800 mV with a total equivalent series resistance (ESR) of 37  $\Omega$  and

113 the highest power recorded of 18 mW (Agnès et al., 2014). These systems show to be  
114 dependent of external biofuel and oxygen supply and their configuration are similar to bio-  
115 batteries (functioning in a static electrolytic cell).

116 Hanashi et al. (2009) and Sode et al. (2016) revisited the challenges of biofuel cell  
117 exploiting the possibility of combining charge pumps and capacitors in order to create a  
118 stand-alone self-powered bio-device. In parallel, in recent research on microbial fuel cells  
119 Santoro et al. developed an internal supercapacitor using the electrode reactions to develop  
120 electrostatically self-rechargeable bioelectrodes (Santoro et al., 2016a, Soavi et al., 2016).

121 Herein, for the first time, a self-fed paper-based biofuel cell integrated at materials  
122 level within an internal self-powered supercapacitor is reported. The glucose  
123 dehydrogenase (GDH) enzymatic anode and BOx enzymatic cathode are used as  
124 supercapacitors bio-electrodes and galvanostatic discharges are performed at currents that  
125 are one order of magnitude higher than what is typical for standard operation of biofuel  
126 cells. In open circuit conditions, the EFC stacking is analogous to that of a charged aqueous  
127 electrochemical double layer capacitor (EDLC) that can be electrostatically discharged at  
128 high current rates and, then, self-recharged by resetting cell in rest, demonstrating the proof  
129 of concept for enzymatic electrodes using quasi-2D microfluidic system. The results of the  
130 galvanostatic test performed in depletion mode and at different pulse times with currents  
131 ranging between  $0.4 \text{ mA cm}^{-2}$  and  $4 \text{ mA cm}^{-2}$  are reported and discussed. Durability tests  
132 for 4200 discharge/self-recharge cycles over a period of 72 hours (3 days) are also  
133 presented.

134 This design opens the possibilities for the development of self-sustained  
135 environmentally friendly hybrid EFCs-supercapacitors (SC-EFC) that can feasibly be used



136 for practical applications, which demand different ranges of power/current density, and  
137 duration of operation such as sensors, *ex-vivo* biomedical devices or other portable devices,  
138 with an autonomy not envisioned before.

139

## 140 **2. Materials and Methods**

141

### 142 **2.1 Bio-electrodes Fabrication and Device Assembly**

143

144 The paper-based biofuel cell was composed by an anode based on glucose  
145 dehydrogenase (GDH) enzyme and by a cathode based on BOx as previously presented  
146 (Ciniciato et al., 2012; Narvaez Villarrubia et al., 2014). On one hand, the cathode was a  
147 dual-layered passive-gas diffusional electrode constituted of a hydrophobic layer that  
148 promoted the flow of oxygen to the catalytic sites and a catalytic layer conformed by the  
149 enzymatic system (schematic shown in figure 1.A). Toray paper (TP) was used as current  
150 collector. On top of it, the hydrophobic layer was pressed, which consisted of Vulcan XC72  
151 carbon black that was teflonized to a 35wt% and is referred as XC35. The loading of this  
152 teflonized carbon over the TP-current collector was  $83\pm 1 \text{ mg cm}^{-2}$  and 263 psi of pressure  
153 was applied for 10 minutes to assemble the hydrophobic layer (TP-XC35 pellet). After the  
154 pellet was formed,  $10 \mu\text{Lcm}^{-2}$  of isopropanol were added in order to increase the  
155 hydrophobic/hydrophilic gradient within the TP-XC35 and increase the oxygen  
156 “breathing” from the atmospheric environment to the catalytic layer (Narvaez Villarrubia  
157 et al., 2014; Santoro et al., 2016b). Subsequently, buckypaper (20 gsm C-Grade MWCNTs  
158 based-paper with BET area of  $33 \text{ m}^2 \text{ g}^{-1}$ ) was pressed on top of the pellet, for additional 5

159 minutes at the same pressure (263 psi) to form the catalytic layer were BOx was deposited.  
160 For this, 80 mg of BOx enzyme was dissolved in 1 ml of phosphate buffer saline (PBS)  
161 0.1M at pH 7.5 and deposited over night (~12 hours) on the electrode at 4 °C (Santoro et  
162 al., 2016b). The electrode had dimensions of 3.5 cm x 3.5 cm (12.25 cm<sup>2</sup>) and the loading  
163 of the buckypaper was roughly 2 mg cm<sup>-2</sup>. Further optimization of the immobilization  
164 process of the enzyme and the fabrication of high performing gas diffusional electrodes  
165 has been proposed (Rojas-Carbonell et. al., 2016).

166 The anode was prepared utilizing nicotinamide adenine dinucleotide  
167 (NAD<sup>+</sup>/NADH) dependent GDH enzyme (schematic shown in figure 1.B). The electrode  
168 consisted of a bucky paper piece (20gsm C-grade MWNTs based-paper with BET area of  
169 33 m<sup>2</sup>g<sup>-1</sup>) with rectangular shape of also 12.25 cm<sup>2</sup> (3.5 cm x 3.5 cm) with a ‘tail’ of 2 cm  
170 length and 1.5 cm width that served as contact to the external circuit. Also in this case, the  
171 buckypaper loading was similar compared to the one used for the cathode (roughly 2 mg  
172 cm<sup>-2</sup>).

173 Methylene green (MG), a mediator for NADH oxidation to NAD<sup>+</sup>, was  
174 electrodeposited as previous research procedure stated (Narváez Villarrubia et al., 2011;  
175 2013; Svobova et al. 2007). Later, 9.93 mg of GDH was dissolved in 496 µl of 95%  
176 Chitosan / 5% MWCNTs and deposited on the electrode overnight (~12 hours) at 4°C  
177 (Narváez Villarrubia et al., 2013, 2014; Svobova et al. 2007). Even though this anode uses  
178 cofactor and mediator to function, its structural design generates higher current densities  
179 when compared to GOx (Narváez Villarrubia et al., 2011; 2013; 2014,).

180 The bio-electrodes were assembled to a quasi-2D capillary-driven microfluidic  
181 system (Mendez et al., 2010; Benner and Petsev, 2013). This was a ‘fan’-shaped paper-

182 based system, introduced in our previous research (Narváez Villarrubia et al., 2014),  
183 consisting of a 3.5 cm × 3.5 cm rectangle appended to a 180°-circular section of 24 cm of  
184 diameter (Grade 1 Whatman filter paper). Both bio-electrodes, placed with the catalytic  
185 layers facing the paper, were stacked on the rectangular section of the paper-‘fan’ (Figure  
186 1). The biocathode was placed on the microfluidic system assuring an aperture for passive  
187 oxygen diffusion from air. Similarly to our previous research, the device was immersed in  
188 an electrolytic solution of glucose 0.1M NAD<sup>+</sup> 1mM and 0.1M KCl dissolved in PBS 0.1M  
189 at pH 7.5.

190

## 191 **2.2 Hybrid Paper-Based EFC-Supercapacitor Characterization**

192 Electrochemical tests were performed on the SC-EFC using a potentiostat (SP-50, Bio-  
193 Logic, France). The capacitive response of the single electrodes and the overall biofuel cell  
194 was investigated utilizing cyclic voltammetry (CV) in two- and three- electrode modes. In  
195 the latter case, Ag/AgCl (3M KCl) was used as reference electrode and placed in the  
196 electrolyte reservoir. Cathode CVs were run by using the cathode as the working electrode  
197 and the anode as counter electrode. For the anode CVs, the cathode was employed as  
198 counter electrode. This permitted to get the voltammetric response of the single electrodes  
199 in-situ, i.e. in the paper-based biofuel cell setup. Anode and cathode CVs were run between  
200 -0.2 V and 0.2 V (vs Ag/AgCl 3M KCl) and 0 V to 0.5 V (vs Ag/AgCl 3M KCl),  
201 respectively. Cell CVs were run between 0 and 0.6 V in 2-electrode mode with the cathode  
202 being the working electrode and the anode the reference and counterelectrode. In the latter  
203 case, cell CVs were also carried out with identical electrodes not loaded with enzymes as  
204 a control.

205 All the CVs were run at scan rate of 5 and 50 mVs<sup>-1</sup>. Energy and power performances of  
206 the enzymatic fuel cell were evaluated by analysis of the cell voltage profiles under  
207 galvanostatic discharge (GLV). GLV discharges of the SC-EFC were performed from  
208 OCV to 0 V at different current densities ( $i_{\text{pulse}}$ ) varying from 0.4 mA cm<sup>-2</sup> to 4 mA cm<sup>-2</sup>.  
209 Ag/AgCl reference electrode was used to monitor the anode and cathode potentials during  
210 discharge. The GLV discharge causes the decrease of the open circuit voltage of the  
211 charged cell ( $V_{\text{max, oc}}$ ) by an ohmic drop ( $\Delta V_{\text{ohmic}}$ ) that is related to the equivalent series  
212 resistance (ESR) of the SC-EFC, to which contribute electrolyte and electrodes resistances.  
213 The ESR is calculated as the ratio between the  $\Delta V_{\text{ohmic}}$  and the pulse current applied ( $i_{\text{pulse}}$ ).  
214 Following the ohmic drop, a capacitive decrease of the voltage over time ( $\Delta V_{\text{capacitive}}$ ) takes  
215 place due to the kinetics of the redox processes and to the capacitive features of the SC-  
216 EFC electrodes. The cell and electrode capacitances (C) were calculated from the ratio  
217 between  $i_{\text{pulse}}$  and the slope (s) in the cell voltage (or electrode potential)-time curve.  
218 Practical values of maximum energy ( $E_{\text{max}}$ ) and power ( $P_{\text{max}}$ ) were evaluated considering  
219 the maximum available voltage after the ohmic drop ( $V_{\text{max}}$ ) calculated as the difference  
220 between the open circuit voltage (OCV) of the charged cell ( $V_{\text{max, oc}}$ ) and  $\Delta V_{\text{ohmic}}$ .  $P_{\text{max}}$  was  
221 obtained multiplying  $i_{\text{pulse}}$  and  $V_{\text{max}}$ . As discussed above, the voltage decreases over the  
222 discharge pulse, along with the practical energy,  $E_{\text{pulse}}$ , which is delivered during the pulse  
223 and which is calculated by the following equation:

224

$$225 \quad E_{\text{pulse}} = i_{\text{pulse}} \int_0^{t_{\text{pulse}}} V dt \quad (1)$$

226

227 where  $t_{\text{pulse}}$  is the pulse time.

228 The pulse power ( $P_{\text{pulse}}$ ) is lower than  $P_{\text{max}}$  and corresponds to  $P_{\text{pulse}} = E_{\text{pulse}} / t_{\text{pulse}}$ , (2)

229

230 **PLEASE INSERT HERE FIGURE 1**

231

### 232 **3. Results and discussion**

233

#### 234 **3.1 Voltammetric Survey**

235

236 **PLEASE INSERT HERE FIGURE 2**

237

238 Figure 2.a compares the voltammograms of the cell with the presence and the absence of  
239 enzymes at  $5 \text{ mV s}^{-1}$  and  $50 \text{ mV s}^{-1}$ . At the highest scan rate, the two cells feature almost  
240 the same cathodic currents, therefore unraveling a similar capacitive behaviour. A  
241 capacitance of  $5.4 \text{ mF cm}^{-2}$  (65 mF) is deduced for both systems dividing the current  
242 density by the scan rate. The main difference between the two cells is evident in the anodic  
243 currents. The enzyme loaded cell exhibits lower currents than the cell without enzymes.  
244 The voltammogram of the former cell deviates from the symmetric box shaped one that is  
245 expected for supercapacitors assembled with high surface area carbon electrodes, and  
246 which in turn is obtained with the no-enzyme cell. Such different behaviour is further  
247 evidenced at the lowest scan rate (Figure 2.a). At  $5 \text{ mV s}^{-1}$ , the faradic and irreversible  
248 processes that characterize the biofuel cell operation, namely glucose oxidation and oxygen  
249 reduction, are driving the CV response of the cell. In order to investigate the contribution  
250 of each electrode to the overall cell response, CVs were performed in 3-electrode mode

251 and the results at  $50 \text{ mV s}^{-1}$  are shown in Figure 2.b. Cathode response is almost symmetric  
252 with currents similar to those featured by the cell. This indicates that cell capacitive  
253 response is dominated by the cathode. In turn, the anode CVs are distorted and above 0.1  
254 V vs Ag/AgCl 3M KCl, a steep increase of the anodic current can be appreciated due to  
255 the onset of glucose oxidation.

256 Figure 2 indicates that at the highest scan rates (and currents), the main contribution to the  
257 cell capacitance is given by the electric double layer formed at the carbonaceous electrodes  
258 interfaces. At the lowest scan rates (and currents), the enzymatic faradic processes, and  
259 specifically ORR, are playing the major role and increase cell capacitance with respect to  
260 the cell without enzymes. The main difference between the cell with and without enzyme  
261 is that, in rest conditions, the open circuit voltage (OCV) of the cell with no enzymes is  
262 around 0 V because it is assembled with identical electrodes experiencing the same  
263 electrolyte with identical environments. The presence of enzymes allowed the cell to  
264 feature an OCV of roughly 600 mV due to the different equilibrium potentials of the redox  
265 processes taking place at the anode and cathode. Consequently, this enables the self-  
266 polarization of the electrodes that can be exploited to design the supercapacitive self-  
267 powered biofuel cell that is discussed in the further sections.

268

### 269 **3.2 Overall and single electrode discharge profiles**

270

271 **PLEASE INSERT HERE FIGURE 3**

272

273 Cell voltage and electrodes potential profiles of the SC-EFC under a discharge at 0.4 mA  
274  $\text{cm}^{-2}$  ( $i_{\text{pulse}}$  of 5 mA) and the following self-recharge is presented in Figure 3.a. Cell voltage  
275 and electrodes potential profiles of the SC-EFC under discharges at different currents and  
276 the following self-recharge are presented in Figure S1. The open circuit voltage of the paper  
277 based biofuel cell was  $563 \pm 14 \text{ mV}$  in agreement with previously presented data. The  
278 cathode open circuit potential (OCP) was  $+496 \pm 4 \text{ mV}$  vs Ag/AgCl (the positive electrode)  
279 and anode OCP was  $-66 \pm 13 \text{ mV}$  vs Ag/AgCl (the negative electrode). These values agree  
280 with previously reported OCP for glucose dehydrogenase and bilirubin oxidase (Narváez  
281 Villarrubia et al., 2013; 2014).

282 The cell voltage linearly decreases during the pulse like in EDLCs. From the slope  
283 of the cell voltage over time at  $i_{\text{pulse}}$  of  $0.4 \text{ mA cm}^{-2}$  a cell capacitance value of  $8.25 \text{ mF}$   
284  $\text{cm}^{-2}$  is obtained. The profiles of the electrodes potentials evidence that cell capacitance is  
285 mainly affected by the positive electrode response. Indeed, while the positive electrode  
286 potential linearly decreases during discharge and exhibits  $9.4 \text{ mF cm}^{-2}$ , the negative  
287 electrode potential increase during the discharge is almost negligible. The positive  
288 electrode capacitance is reasonably low because of the low surface area ( $33 \text{ m}^2 \text{ g}^{-1}$ ) and low  
289 carbon loading ( $2 \text{ mg cm}^{-2}$ ) of the buckypaper. On the other hand, the capacitive response  
290 of the negative electrode, with exactly the same surface area and loading of the positive  
291 electrode, is much higher and was measured as  $67 \text{ mF cm}^{-2}$ .

292 This suggests that while during discharge the positive electrode behaved like a  
293 conventional EDLC positive electrode, the negative electrode responded by a fast redox  
294 process, namely the oxidation of glucose by the enzymatic process. Hence, at such high  
295 current response, the SC-EFC operates like a hybrid supercapacitor, i.e. a capacitor with a

296 positive electrode working by an electrostatic process and a negative electrode working by  
297 a Faradic process. Note that, this is highlighted by the anode CV reported in Figure 2b, in  
298 which glucose oxidation is not reversible. Therefore, for sake of clarity, we would like to  
299 underline that the negative electrode cannot be termed “pseudocapacitive” as it would be  
300 in a conventional hybrid supercapacitor.

301 At  $0.4 \text{ mA cm}^{-2}$  the full discharge time was  $\approx 9.1 \text{ s}$  followed by a  $\approx 16 \text{ s}$  recharge  
302 obtained without the utilization of any external device (Figure 3.a). Indeed, during the rest  
303 period in open circuit after the pulse, electrode potentials moved back to their initial  
304 equilibrium values and cell voltage was restored to the value exhibited before the pulse.  
305 The EFC was, then, tested at higher current densities ( $0.8$  to  $4 \text{ mA cm}^{-2}$ ), and the cell  
306 voltage (Figure 3.b) and electrodes potential (Figure 3.c) profiles for  $i_{\text{pulse}}$  ranging from  $0.8$   
307  $\text{mA cm}^{-2}$  to  $4 \text{ mA cm}^{-2}$  are reported.

308 As expected, the discharge time decreased with the increase of the  $i_{\text{pulse}}$ . The  
309 complete discharge of the supercapacitor took place in  $\approx 9.1 \text{ sec}$  at  $0.4 \text{ mA cm}^{-2}$  (Figure 3.a)  
310 and  $0.053 \text{ sec}$  at  $4 \text{ mA cm}^{-2}$  applied (Figure 3.b). Cell voltage profiles were shaped by the  
311 different rate response of positive and negative electrode. The positive electrode potential  
312 profiles were mainly affected by electrode capacitive behavior while the negative electrode  
313 potential profiles were mainly affected by the ohmic drop, i.e. by negative electrode  
314 resistance. In fact, the overall ESR was  $6 \Omega$  ( $0.49 \Omega \text{ cm}^2$ ) in which  $4 \Omega$  ( $0.33 \Omega \text{ cm}^2$ ) and  $2$   
315  $\Omega$  ( $0.16 \Omega \text{ cm}^2$ ) were due to negative electrode and positive electrode respectively. Indeed,  
316 at the lowest current investigated ( $0.4 \text{ mA cm}^{-2}$ ), the positive electrode ohmic drop was  
317 only of  $\approx 10 \text{ mV}$ , to be compared to  $\approx 20 \text{ mV}$  for the negative electrode (Figure 3.a). During  
318 the complete discharge, the voltage decrease of the positive electrode was  $\approx 478 \text{ mV}$ , much



319 higher compared to the voltage decrease of the negative electrode  $\approx 77$  mV. At the highest  
320 current investigated ( $4 \text{ mA cm}^{-2}$ ), the positive electrode ohmic drop was only of  $\approx 100$  mV,  
321 to be compared to  $\approx 200$  mV for the negative electrode. The voltage decrease of the positive  
322 electrode during the pulse ( $4 \text{ mA cm}^{-2}$ ) was  $\approx 160$  mV and much higher than that of the  
323 negative electrode ( $\approx 40$  mV). Hence,  $\Delta V_{\text{ohmic}}$  of the cell was mainly affected by the  
324 negative electrode (which mainly contributes to cell ESR) while the  $\Delta V_{\text{capacitive}}$  of the cell  
325 was mainly affected by the positive electrode.

326         Additionally, negative electrode and positive electrode contribute differently to cell  
327 response under short and long-time pulses. At short time (10 ms) pulses, the cell  
328 performance is mainly affected by the ohmic drop, which in turn mainly depends on the  
329 negative electrode. Instead, at longer times, cell performance is influenced by the  
330 capacitive response of the positive electrode.

331         The curves reported in Figure 3 were used to evaluate cell performance at very short  
332 and at longer time pulse response. The maximum power is calculated on the basis of the  
333 cell ESR and does not consider the capacitive behavior, hence it is representative of the  
334 short time response of the cell.  $E_{\text{pulse}}$  and  $P_{\text{pulse}}$  are calculated considering the complete  
335 discharge profile over the entire pulse duration. Thus, they represent the practical cell  
336 performance at different time pulses and pulse currents.

337

### 338 **3.3 Power Curves and Ragone Plot**

339

340

341 **PLEASE INSERT HERE FIGURE 4**

342

343  $P_{\max}$  was calculated at different current densities considering  $V_{\max}$  of 0.56 V and  
344 ESR of  $6 \Omega$  (Figure 4.a). The highest value of  $1.07 \text{ mW cm}^{-2}$  (13.1 mW) was measured for  
345 current pulse of  $3.6 \text{ mA cm}^{-2}$ . This value is one order of magnitude higher than the power  
346 obtained by the biofuel cell in stationary operation (Narváez Villarrubia et al., 2014).  
347 Figure 4.a also reports the  $P_{\text{pulse}}$  for different  $t_{\text{pulse}}$  of 1, 0.5, 0.25, 0.1 and 0.01 sec at  
348 different currents. As expected,  $P_{\text{pulse}}$  decreases with the increase of time due to the  
349 capacitive response of the cell which decreases the cell voltage over time. The highest value  
350 of  $P_{\text{pulse}}$  was  $0.27 \text{ mW cm}^{-2}$  for  $t_{\text{pulse}}$  of 1 s,  $0.387 \text{ mW cm}^{-2}$  for  $t_{\text{pulse}}$  of 0.5 s,  $0.509 \text{ mW cm}^{-2}$   
351  $^2$  at  $t_{\text{pulse}}$  for 0.25 s,  $0.66 \text{ mW cm}^{-2}$  for  $t_{\text{pulse}}$  of 0.1 s, and  $0.868 \text{ mW cm}^{-2}$  for  $t_{\text{pulse}}$  of 0.01 s.

352 The values of  $E_{\text{pulse}}$  and  $P_{\text{pulse}}$ , for complete discharges, from  $V_{\max, \text{OC}}$  to 0V, at  
353 different currents were used to build the Ragone plot reported in Figure 4.b. The highest is  
354 the current, the lower is  $E_{\text{pulse}}$  and the highest is  $P_{\text{pulse}}$ .

355 The highest energy and power densities for complete discharges are  $0.177 \mu\text{Wh cm}^{-2}$   
356  $^2$  ( $0.4 \text{ mA cm}^{-2}$ , 9.015 s) and  $393 \mu\text{W cm}^{-2}$  ( $3.2 \text{ mA cm}^{-2}$ , 0.141 s) respectively. Complete  
357 discharges of ca. 0.5 s ( $1\text{-}2 \text{ mA cm}^{-2}$ ) provide the best matching for  $P_{\text{pulse}}$  ( $200\text{-}300 \mu\text{W cm}^{-2}$   
358  $^2$ ) and  $E_{\text{pulse}}$  ( $0.04\text{-}0.05 \mu\text{Wh cm}^{-2}$ ).

359 Durability tests over 3 days (4200 cycles) have been conducted and presented in  
360 the supporting information [Figure S2]. The results indicated a slight decrease in working  
361 open circuit voltage (OCV) and cell capacitance over time [Figure S2].

362

### 363 **3.5 Outlook**

364

365 For the first time, a self-fed paper based biofuel cell was used as hybrid self-powered  $\mu$ -  
366 supercapacitor which delivers significant power under short and high current pulses  
367 compared to conventional EFC operation. In this case, positive electrode responded using  
368 an electrostatic process while the negative electrode worked using a Faradic process like  
369 in a hybrid supercapacitor. The particular configuration of EFC allows a continuous and  
370 constant biofuel supply through capillary-driven flow, electrolytes and products of reaction  
371 through the quasi-2D microfluidic system. Differently to previous studies (Pankratov et al.  
372 2014a; 2014b; 2014c; Agnes et al., 2014), in this research oxygen was not actively supplied  
373 in the electrolyte. Furthermore, electrolyte was wetting electrode exploiting capillarity,  
374 which might explain the lower cathode capacitive performances registered. In fact, the  
375 passive diffusion of oxygen from air to the three phase interface of the catalytic layer of  
376 the cathode is driven by a concentration gradient in the hydrophilic/hydrophobic layers  
377 formed with the specific configuration of this biocathode. High capacitive response  
378 requires that the high surface area of the carbon is entirely wetted with the electrolytic  
379 solution. The main advantage of the paper-based biofuel cell / supercapacitor integrated  
380 system lays in the fact that this system is self-powered and self-sustained; it could work  
381 until complete depletion of biofuel, using no other external power source. This work  
382 demonstrates the feasibility of using selective enzymatic electrodes as electrochemical  
383 storage systems (i.e. supercapacitors) in a hybrid device that could work independently  
384 from external energy sources. Further studies should be completed in the utilization of  
385 amplified and pulsed signals into sensors development, or conformations to power *ex-vivo*  
386 biomedical devices or portable devices.

387

388 **4. Conclusions**

389

390 A glucose/air paper-based biofuel cell / supercapacitor integrated system was demonstrated  
391 with NAD<sup>+</sup>/NADH-dependent glucose dehydrogenase and bilirubin oxidase enzymes  
392 employed at the anode and cathode, respectively. The paper-based microfluidic device  
393 allowed self-feeding of glucose (biofuel) and oxygen (oxidant) to the cell. The system has  
394 very low equivalent series resistance quantified in 6 Ω. The supercapacitive features of the  
395 electrodes generated short and high current pulse discharge up to 4 mAcm<sup>-2</sup>. The practical  
396 power achieved was 1.07 mW cm<sup>-2</sup> (13.1 mW), which is among the highest power ever  
397 recorded for this kind of hybrid systems. A maximum pulse power of 0.87 mWcm<sup>-2</sup> (10.64  
398 mW) was measured for pulses of 0.01 s. The capacitive features of the nanostructured  
399 electrodes integrated in a 'fan' paper-based biofuel cell configuration enabled current and  
400 power densities at least one order of magnitude higher than compared to steady state mode.  
401 The SC-EFC cathode was limiting cell capacitance and improvements are expected by the  
402 use of a carbonaceous substrate of higher specific surface area. Utilization of carbon  
403 materials featuring at least 1000 m<sup>2</sup> g<sup>-1</sup> could raise electrode response in the order of Farads,  
404 and increase pulse energy by 1-2 order of magnitude.

405

406 **Acknowledgement**

407

408 FS and CA acknowledge financial support by Alma Mater Studiorum - Università di  
409 Bologna (Researcher Mobility Program).

410

411 **References**

412

413 Agnès, C., Holzinger, M., Le Goff, A., Reuillard, B., Elouarzaki, K., Tingry, S., Cosnier  
414 S., 2014. *Energy Environ. Sci.* 7, 1884-1888

415 Amir, L., Tam, T.K., Pita, M., Meijler, M.M., Alfonta, L., Katz, E., 2009. *J. Am. Chem.*  
416 *Soc.* 131, 826-832.

417 Atanasov, P., Apblett, C., Brozik, S., Calabrese Barton, S.; Cooney, M., Liaw, B. Y.,  
418 Mukerjee, S., Minteer, S. D. 2007. *Electrochem. Soc. Interface.* 16, 28–31.

419 Béguin, F., Presser, V., Balducci, A., Frackowiak, E., 2014. *Adv. Mater.* 26(14), 2219-  
420 2251

421 Benner, E., Petsev, D.N., 2013. Potential flow in the presence of a sudden expansion:  
422 Application to capillary driven transport in porous media. *Phys. Rev. E* 87 (033008),  
423 1-10.

424 Ciniciato, G.P.M.K., Lau, C., Cochrane, A., Sibbett, S.S., Gonzalez, E.R., Atanassov, P.,  
425 2012. *Electroc. Acta* 82, 208-213.

426 Conway, B.E., 1999. *Electrochemical Supercapacitors: Scientific Fundamentals and*  
427 *Technological Applications*, Springer.

428 Cooney, M.J., Lau, C., Windmeisser, M., Liaw, B.Y., Klotzbach, T., Minteer, S.D., 2008.  
429 *J. Mater. Chem.* 6, 667-674.

430 Cosnier, S., Holzinger, M., Le Goff, A. 2008. *Front. Bioeng. Biotechnol.*, 2(45), 1-5.

431 Davis, F., Higson, S.P.J., 2007. *Biosens. Bioelectron.* 22, 224-1235.

432 Desmet, C., Marquette, C. A., Blum, L. J., Doumèche, B., 2016. *Biosens. Bioelectron.* 76,  
433 145–163.

434 Falk, M., Narvaez Villarrubia, C.W., Babanova, S., Atanassov, A., Shleev, S., 2013.  
435 ChemPhysChem 14(10), 2045-2058.

436 Garcia, S. O., Ulyanova, Y. V., Figueroa-Teran, R., Bhatt, K. H., Singhal, S., Atanassov, P., 2016.  
437 ECS J. Solid State Sci. Tech. 5 (8) M3075-M3081.

438 Gellett, W., Schumacher, J., Kesmez, M., Le, D., Minter, S.D., 2010. J. Electrochem. Soc.  
439 157 (4), B557-B562.

440 González-Arribas, E., Pankratov, D., Gounel, S., Mano, N., Blum, Z., Shleev, S., 2016.  
441 Electroanalysis. doi: 10.1002/elan.201600096

442 González-Guerrero, M.J., Esquivel, J.P., Sánchez-Molas, D., Godignon, P., Xavier Muñoz,  
443 F., del Campo, F.J., Giroud, F., Minter, S.D. Sabate, N., 2013. Lab Chip 13, 2972.

444 Gupta, G., Rathod, S.B., Staggs, K.W., Ista, L.K., Oucherif, K.A., Atanassov, P.B., Tartis,  
445 M.S., and Montano, G.A., Lopez, G.P., 2009. Langmuir 25(23), 13322-13327.

446 Hanashi, T., Yamazaki, T., Tsugawa, W., Ferri, S., Nakayama, D., Tomiyama, M.,  
447 Ikebukuro, K., Sode, K., 2009. Biosens Bioelectron. 24, 1837-1842

448 Heller, A., 1992. J.Phys. Chem. 96, 3579-3587.

449 Ivnitski, D., Artyushkova, K., Rincón, R.A., Atanassov, P., Luckarift, H.R., Johnson, G.R.,  
450 2008. Small 4, 357-364.

451 Kang, C., Shin, H., Heller, A., 2006. Bioelectrochem. 68(1), 22-26.

452 Kizling, M., Draminska, S., Stolarczyk, K., Tammela, P., Wang, Z., Nyholm, L., Bilewicz,  
453 R., 2015. Bioelectrochem. 106, 34-40.

454 Lau, C., Moehlenbrock, M. J., Arechederra, R. L., Falase, A., Garcia, K., Rincon, R.,  
455 Minter, S. D., Banta, S., Gupta, G., Babanova, S., Atanassov, P. 2015. Int. J.  
456 Hydrogen Energy 40, 1461-1466.

457 Li, S., Wang, Y., Ge, S., Yu, S., Yan, M., 2015. *Biosens. Bioelectron.* 71, 18–24.

458 Majdecka, D., Bilewicz, R., 2016. *J. Solid State Electrochem.* 20, 949–955.

459 Mano, N., Mao, F., Shin, W., Chen, T., Heller, A., 2003. *Chem. Comm.*, 518-519.

460 Mendez, S., Fenton, E.M., Gallegos, G.R., Petsev, D.N., Sibbett, S.S., Stone, H.A., Zhang,  
461 Y., López, G.P., 2010. *Langmuir* 26, 1380-1385.

462 Minteer, S.D., Liaw, B.Y., Cooney, M.J., 2007. *Curr. Opin. Biotech.* 18, 228 - 234.

463 Minteer, S.D., 2012a. *Top. Catal.* 55, 1157-1161.

464 Minteer, S.D., Atanassov, P., Luckarift, H.R., Johnson, G.R., 2012b. *Mater. Today* 15(4),  
465 166-173.

466 Moore, C.M., Minteer, S.D., Martin, R.S., 2005. *Lab Chip* 5, 218-225.

467 Narváez Villarrubia, C.W., Rincon, R.A., Radhakrishnan, V.K.; Davis, V., Atanassov, P.,  
468 2011. *ACS App. Mater. Interfaces* 3, 2402-2409.

469 Narváez Villarrubia, C.W., Garcia, S.O., Lau, C., Atanassov, P., 2013. *ECS J. Solid State*  
470 *Sci. Technol.* 2(10), M3156-M3159.

471 Narváez Villarrubia, C.W., Lau, C., Ciniciato, G.P.M.K., Garcia, S.O., Sibbett, S.S.,  
472 Petsev, D.N., Babanova, S., Gupta, G., Atanassov, P., 2014. *Electrochem. Comm.* 45,  
473 44-47.

474 Pardo-Yissar, V., Katz, E., Willner, I., Kotlyar, A.B., Sanders, C., Lill, H., 2000. *Farad.*  
475 *Discuss.* 116, 119-134.

476 Pankratov, D., Blum, Z., Shleev, S., 2014a. *ChemElectroChem* 1, 1798 - 1807.

477 Pankratov, D., Falkman, P., Blum, Z., Shleev, S. *Energy Environ. Sci.* 2014b, 7, 989-993.

478 Pankratov, D., Blum, Z., Suyatin, D.B., Popov V.O., Shleev, S., 2014c. *ChemElectroChem*  
479 1(2), 343-346.

480 Rasmussen, M., Abdellaoui, S., Minteer, S. D. 2016. *Biosens. Bioelectron.*, 76, 91-102.

481 Reid, R.C., Giroud, F., Minteer, S.D., Galea, B.K., 2013. *J. Electrochem. Soc.* 160 (9),  
482 H612-H619

483 Rincón, R.A., Lau, C., Garcia, K.A., Atanassov, P., 2011. *Electrochim. Acta* 56, 2503-  
484 2509.

485 Rojas-Carbonell, S., Babanova, S., Serov, A., Ulyanova, Y., Singhal, S., Atanassov, P.,  
486 2016. *Electrochim. Acta*, 190, 504-510.

487 Santoro, C., Soavi, F., Serov, A., Arbizzani, C., Atanassov, P., 2016a. *Biosens.*  
488 *Bioelectron.* 78, 229-235

489 Santoro, C., Babanova, S., Erable, B., Schuler, A., Atanassov, P., 2016b. *Bioelectrochem.*  
490 108, 1-7.

491 Shitanda, I., Kato, S., Hoshi, Y., Itagaki, M., Tsujimura, S., 2013. *Chem. Commun.* 49  
492 (94), 11110–11112.

493 Skunik-Nuckowska, M., Grzejszczyk, K., Stolarczyk, K., Bilewicz R., Kulesza, P.J. 2014.  
494 *J. Appl. Electrochem.* 44, 497-507.

495 Slaughter, G., Kulkarni, T., 2015. *Biochip. Tissue Chip* 5(1), 1-10.

496 Slaughter, G., Kulkarni, T., 2016. *Biosens. Bioelectron.* 78, 45-50.

497 Soavi, F., Bettini, L.G., Piseri, P., Milani, P., Santoro, C., Atanassov, P., Arbizzani, C.,  
498 2016. *J. Power Sources.* doi:10.1016/j.jpowsour.2016.04.131

499 Sode, K., Yamazaki, T., Lee, I., Hanashi, T., Tsugawa, W., 2016. *Biosens. Bioelectron.* 76,  
500 20–28.

501 Sokic-Lazic, D., Minteer, S.D., 2008. *Biosensens. Bioelectron.* 24, 939-944.

502 Soukharev, V., Mano, N., Heller, A., 2004. *J. Am. Chem. Soc.* 126(27), 8368-8369.



- 503 Southcott, M., MacVittie, K., Halánek, J., Halámková, L., Jemison, W. D., Lobel, R., Katz,  
504 E., 2013. *Phys.Chem.Chem.Phys.* 15, 6278-6283.
- 505 Strack, G., Babanova, S., Farrington, K. E., Luckarift, H. R., Atanassov, P., Johnsona, G. R., 2013.  
506 *J. Electrochem, Soc.* 160 (7), G3178-G3182.
- 507 Svoboda, V., Cooney, M.J., Rippolz, C., Liaw, B.Y., 2007. *J. Electrochem. Soc.* 154(3),  
508 D113 - D116.
- 509 Tam, T.K., Pita, M., Ornatska, M., Katz, E., 2009. *Bioelectrochem.* 76(1-2), 4-9.
- 510 Tarasevich, M.R. Bogdanovskaya, V.A. Zagudaeva, N.M., Kapustin, A.V., 2002. *Russ. J.*  
511 *Electrochem.* 38 (3), 335.
- 512 Yu, E.H., Scott, K., 2010. *Energies* 2010, 3, 23.

## Figure Caption

Figure 1. A) Schematic of cathode fabrication, pressing process and BOx deposition. B) Schematic of anode fabrication, MG electrochemical deposition and GDH/Chitosan/CNTs mixture deposition. C) Paper-based EFC assembly, stacking of the cellulose paper-based microfluidic system. D) Paper-based SC-EFC using GDH and BOx as anode and cathode assembled to a quasi-2D microfluidic system inserted in a glucose 0.1M, 1 mM NAD<sup>+</sup> and KCl 0.1M in PB 0.1M at pH 7.5. E) Schematic of self-powered SC-EFC employing GDH anode and BOx cathode used as negative and positive electrodes of the internal supercapacitor, respectively.

Figure 2. Cell CVs with and without enzymes at scan rate of 5 mVs<sup>-1</sup> and 50 mVs<sup>-1</sup> (2-electrode mode) (a). Anode and cathode CVs at scan rate of 50 mVs<sup>-1</sup> (b) (3-electrode mode).

Figure 3. a) Cell voltage and electrodes potential profiles of the SC-EFC under a discharge at 0.4 mA cm<sup>-2</sup> and the following rest period. b) Cell voltage and c) positive and negative electrode potential profiles during discharges at different current densities between 0.8 and 4 mA cm<sup>-2</sup>.

Figure 4. a) Power curves at different current pulses. b) Ragone plot of the SC-EFC.

Figure 1

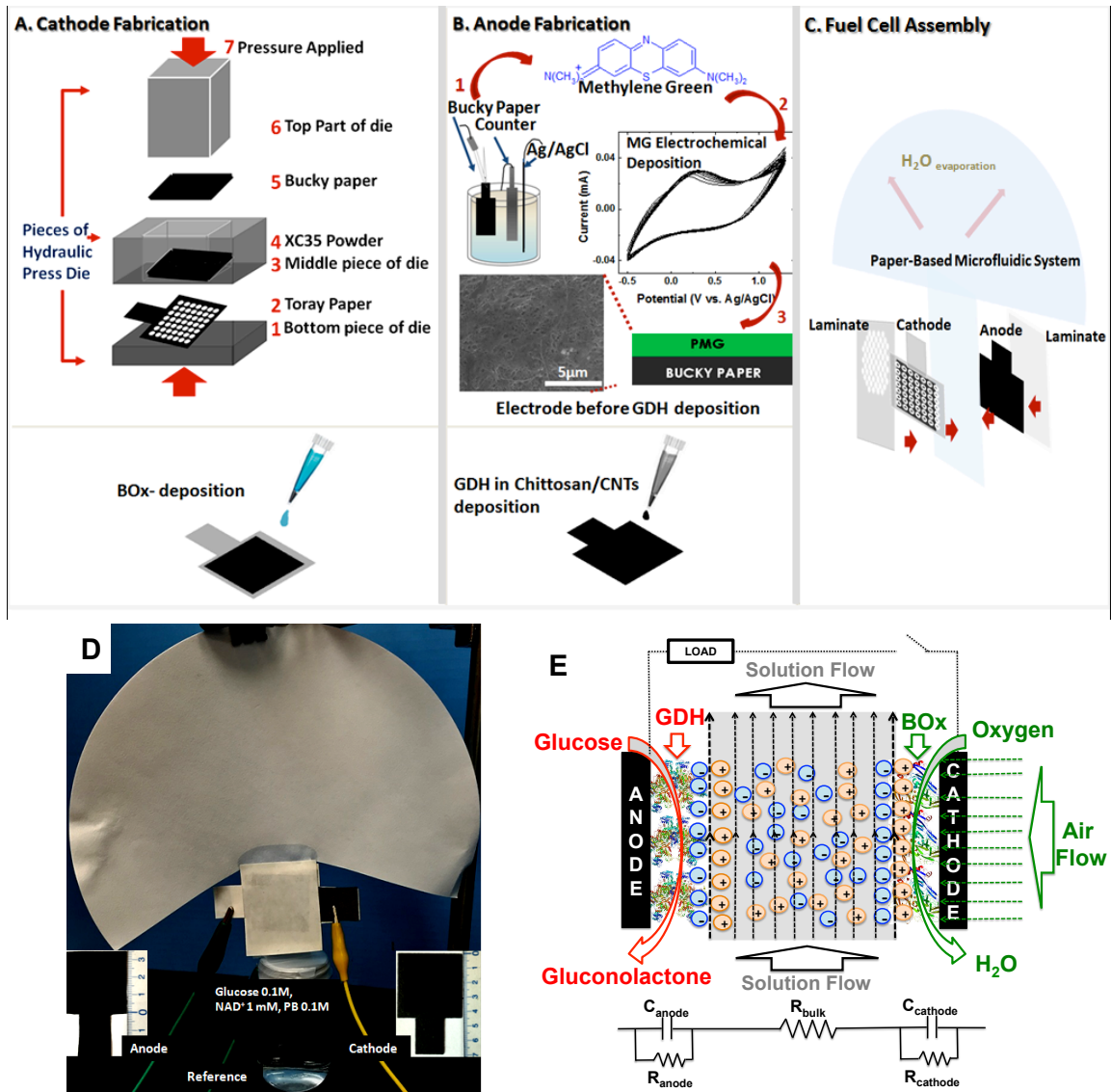


Figure 2

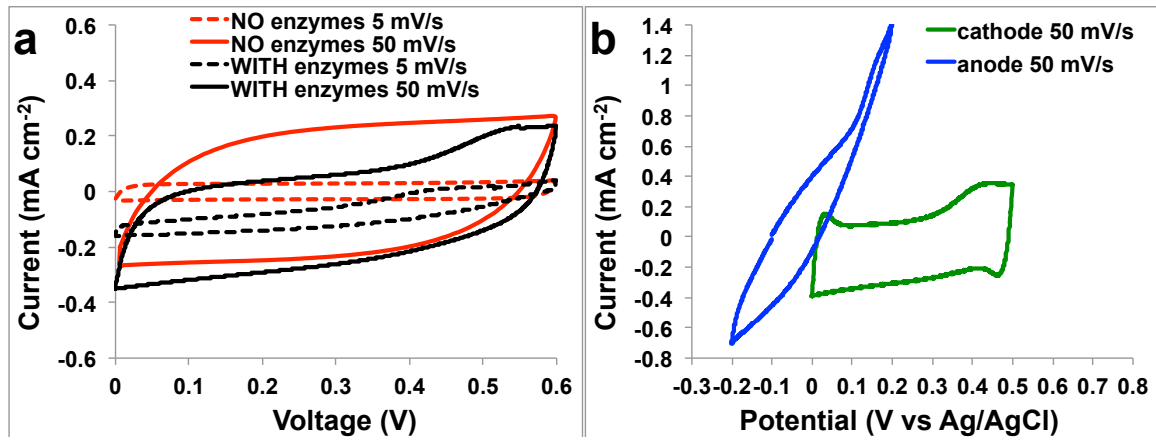


Figure 3

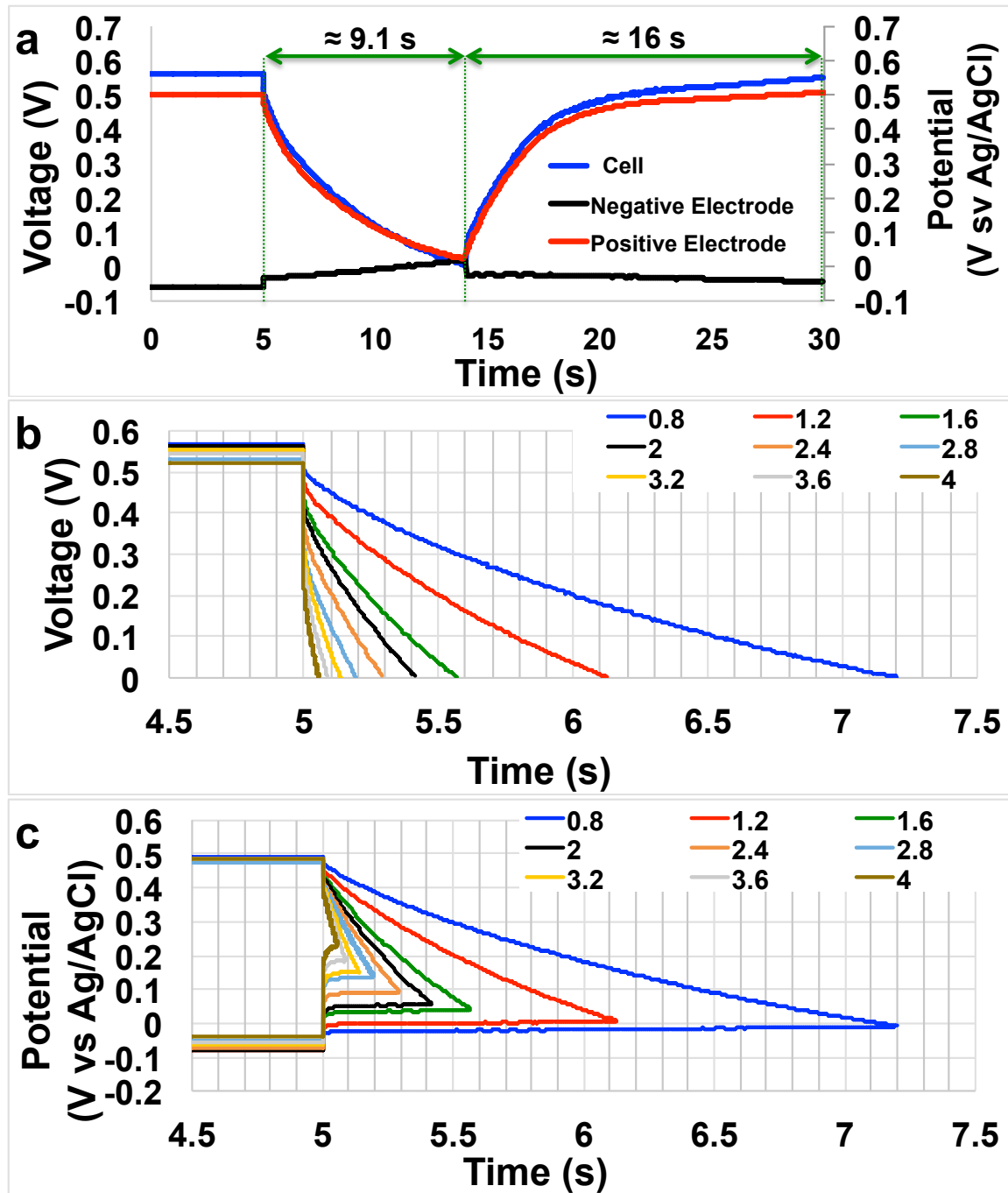


Figure 4

